Heliyon 9 (2023) e12923

Contents lists available at ScienceDirect

Heliyon

journal homepage: www.cell.com/heliyon

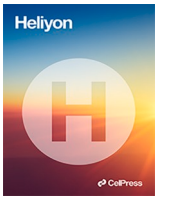

Research article

Biomechanical analysis of customized cage conforming to the endplate morphology in anterior cervical discectomy fusion: A finite element analysis

Bin Sun, Qing Han, FengXu Sui, AoBo Zhang, Yang Liu, Peng Xia **, JinCheng Wang, XiaoYu Yang *

Department of Orthopedics, The Second Hospital of Jilin University, No. 218 Ziqiang Street, 130041, Changchun, Jilin, China

ARTICLE INFO

Keywords:
Biomechanical
Cervical
Cage
ACDF
Finite element analysis

ABSTRACT

In anterior cervical discectomy and fusion (ACDF), an interbody fusion device is an essential implant. An unsuitable interbody fusion device can cause postoperative complications, including subsidence and nonunion. We designed a customized intervertebral fusion device to reduce postoperative complications and validated it by finite element analysis. Herein, we built a non-homogeneous model of the C3-7 cervical spine. Three implant models (customized cage, commercial cage, and bone graft cage) were constructed and placed in the C45 cervical segment after ACDF surgery. The simulated range of motion (ROM), stress at the cage-bone interface, and stress on the cage and implants were compared under different conditions. The commercial cage showed maximum stress peaks at 40.3 MPa and 43.2 MPa in the inferior endplate of C4 and superior endplate of C5 under rotational conditions, higher compared to 29.7 MPa and 26.4 MPa, respectively, in the customized cage. The ROM was not significantly different between the three cages placed after ACDF. The stresses on the commercial cage were higher compared to the other two cages under all conditions. The bone graft in the customized cage was subject to higher stress than the commercial cage under all conditions, particularly lateral bending, wherein the maximum stress was 5.5 MPa. These results showed that a customized cage that better conformed to the vertebral anatomy was promising for reducing the risk of stress shielding and the occurrence of subsidence.

1. Introduction

Anterior discectomy and fusion (ACDF) surgery is widely performed for the treatment of cervical disc disease, like cervical spondylotic myelopathy, cervical disc herniation, and posterior longitudinal ligament ossification [1,2]. An intervertebral fusion device for fixation is the most commonly used in this surgery and plays an important role in restoring disc height, decompressing, and maintaining stability [3,4]. However, complications, including non-healing bone, subsidence, and pseudoarthrosis occur after surgery [5,6]. Although various new fusion devices have been developed and used in clinical settings, postoperative complications have not improved significantly.

* Corresponding author.
** Corresponding author.
E-mail addresses: xiapeng@jlu.edu.cn (P. Xia), yangxiaoy@jlu.edu.cn (X. Yang).

https://doi.org/10.1016/j.heliyon.2023.e12923
Received 8 September 2022; Received in revised form 28 December 2022; Accepted 9 January 2023
Available online 12 January 2023

Inappropriate moduli of elasticity or mismatches in the shape of the intervertebral fusion device are essential factors during the subsidence [7– 9]. Optimizing intervertebral fusion devices by changing their material properties and constructing for microporosity are favorable research directions. The advent of the cage in materials like titanium and poly-ether-ether-ketone (PEEK) has gradually replaced autologous bone grafts and become mainstream, owing to the better stability and biocompatibility of titanium alloys; the elastic modulus of PEEK is close to that of cortical bone [10,11]. Wang et al. [12] performed local topological optimization of the unit lattice to obtain a lattice structure filled into the lumbar fusion for microporous fusion, which reduced the weight and showed a more uniform stress distribution. Although altering the elastic modulus of the intervertebral fusion cage improves the stress distribution across the vertebral body, decisive help in resolving postoperative subsidence remains lacking.

In addition to changing the elastic modulus properties, the shape design of the intervertebral fusion is popular for optimization. However, the majority of intervertebral fusion shapes are designed with emphasis only on contact area, intervertebral height restoration, intervertebral fusion fixation, and form fixation parameters. Despite the convenience of commercially available cages designed according to fixation parameters, the vertebral structure of individual patients is different, leading to neglecting of individualized characteristics of commercial cages, and ineffective results after application. Recently, the concept of personalization has been gradually developed with the integration of bionic and biomechanical concepts into the design of implants and gained traction [13]. Kang et al. [14] designed a multisegmented artificial intervertebral implant customized to the patient's spinal anatomy, which not only met the safety requirements of the implant but also achieved positive clinical results. The customized design provided better matching of the cage-bone interface, improved biomechanics, and a homogeneous mechanical distribution of the vertebral body surface along with reasonable mechanical conduction. Therefore, designing a cage that can conform to suit the individual patient's requirements and simultaneously reduce postoperative complications is necessitated.

Finite element analysis (FEA) simulates the biomechanics of a model, thus making up for the lack of experimental biomechanical data from in vitro experiments. Application in spinal surgery also has the advantages of convenient modeling, the possibility of constructing different procedures, and adjusting the applied forces. Therefore, FEA is a crucial tool for solving complex problems in the biomechanical study of the spine. In this work, a finite element model of the healthy human cervical spine C3–C7 was established, which was modified such that an intervertebral fusion cage could be inserted in the C4–C5 segment during ACDF operation. We attempted to use an individualized cage design method to reduce the risk of cage sinking and stress shielding. Therefore, the purpose of this study was to analyze the impact of different cages on the biomechanics of the affected and adjacent segments after surgery.

2. Material and methods

2.1. Models

The computer tomography (CT) thin-section scans of the cervical spine were obtained from normal healthy female volunteers aged 32 years (height: 172 cm, weight: 70 kg, and thickness: 0.625 mm). The study design was approved by the Ethics Committee of the Second Hospital of Jilin University, and informed consent was obtained from the volunteers. Subsequently, the CT scan images were imported into Mimics (Mimics 19, Materialise, Inc., Belgium) software, the thresholds were adjusted to visualize the areas of C3-7 bones, a layered examination was performed to show the unrecognized and redundant parts of the system, and after obtaining the 3D model, it was smoothed and the noise was reduced. Cortical and cancellous bones were assigned using the gray value formula in

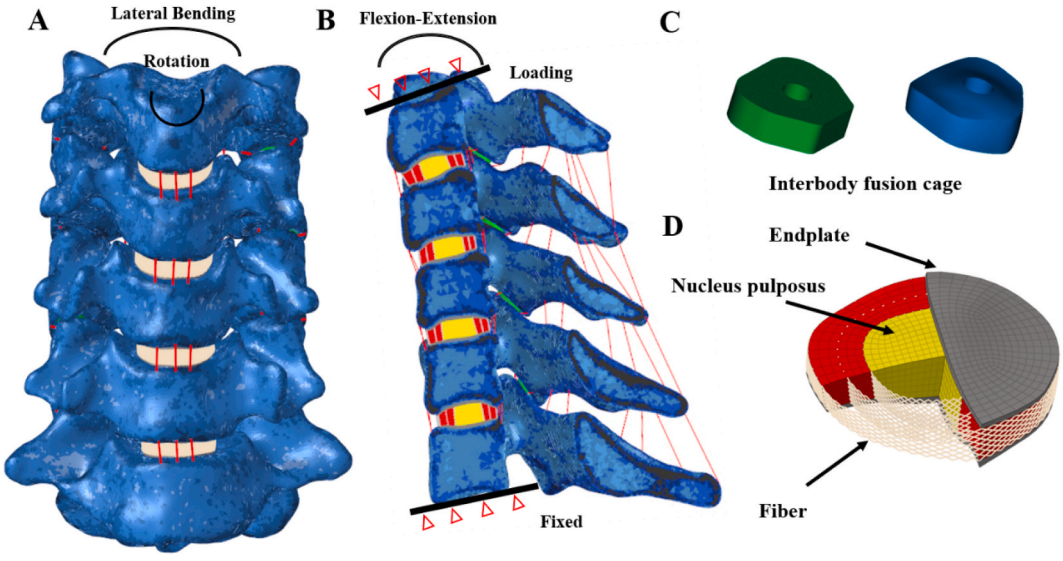

Fig. 1. Finite element model for intact C3-7 cervical spine. (A) Intact Model; (B) Force and Constraint; (C) Cage, and (D) Endplate, Nucleus pulposus, and Fiber.

Mimics, and intervertebral disks and cartilage were built using 3-Matic (3-Matic 11.0, Materialise, Inc, Belgium). Finally, the model was imported into Hypermesh 20.0 (Hypermesh 20.0, Altair Technologies, Inc., CA, USA) for meshing, defining material properties, and FEA.

The intact vertebral body comprised cancellous bone, cortical bone, end-plate, intervertebral disc, anterior longitudinal ligament, posterior longitudinal ligament, interspinous ligament, ligamentum flavum, and capsular ligament (Fig. 1A and B). Cortical and cancellous bones were assigned seven different thresholds using the gray value formula. The intervertebral disc comprised the three following parts: nucleus pulposus, annulus ground substance, and annulus fibrosus. The annulus fiber was a net structure consisting of truss units subjected only to tension and inclined between 15° and 45° from the horizontal (Fig. 1D). Diagonal corners of the hexahedra of the fiber annulus were connected using rod units, adjusted to the desired angle, and three layers were built from the medullary nucleus to the outermost side. The hyperelastic material property was assigned to the nucleus pulposus and annulus ground substance. We built a layer of articular cartilage in the joint space of the vertebral body surface using a hexahedral unit. The mesh element size of the C3-7 spine vertebra model was 0.5 mm. To insulate the results of the FEA from the mesh size, 0.3 mm and 0.7 mm meshes were added and set to low quality (element size 0.7 mm, elements 575,103, and nodes 118,692), medium (element size 0.5 mm, elements 1,086,295, and nodes 219,103), and high quality (element size 0.3 mm, elements 3,065,174, and nodes 602,772) meshes, respectively, to perform mesh convergence analysis. The difference between the medium and high-quality models was less than 5%, and thus, the medium-quality mesh was convergent [15]. A layer of articular cartilage was built on the surface of each vertebral body in the facet joint. All five ligaments were built using spring units in the vertebral body. The materials properties for finite element models are listed in Table 1 [16–18].

2.2. Design of the cage

The design of the new customized cage conformed to the anatomy of the human vertebral body based on a bionic concept adhering to the anatomy of the cervical intervertebral space (Fig. 1C). The upper and lower ends of the customized cage fit the same area as that of the lower surface of the C4 vertebra and the upper surface of the C5 vertebra, respectively, thus maximizing the fit to the vertebral body. The area of the customized cage was 40% of the vertebral body surface for providing adequate support. Customized cages with several aspect ratios were created to select the most suitable size, not interfering with the pedicle joint. In the center of the customized cage, holes were designed through the upper and lower curves to allow the insertion of bone grafts for better fusion. The bone cage used the unpunched fitted cage and replaced the material properties with the bone graft material, while the commercial cage used the scanned STL file for reconstruction.

2.3. Simulation of ACDF

The commercial cage was reconstructed by scanning, followed by input into the computer, and the customized cage was fitted according to the top and bottom of the endplate (Fig. 2A). Bone graft cage was simulated by iliac bone extraction. After ACDF surgery, cage subsidence can produce spinal stenosis, causing nerve root pain and nerve root palsy, thus seriously affecting postoperative nerve root decompression. Post-ACDF nerve root palsy is most common in the C4-5 segment. To simulate ACDF surgery, the C4/5disc, superior endplate of C5, inferior endplate of C4, C4/5 anterior longitudinal ligament, and C4/5 posterior longitudinal ligament were removed. The commercial cage, customized cage, and bone graft cage were correspondingly assembled with the surgical model, to simulate the implantation of the cage filled with bone graft (Fig. 2B). We selected the cage-bone interface, cage, and bone graft with von Mises stress as the object to compare the biomechanical effects of the three different cages.

2.4. Boundary, contact and loading conditions

A load of 73.6 N was applied to the upper surface of the C3 vertebral body to simulate the physiological state and a moment of 1 Nm was used to simulate flexion, extension, lateral bending, and axial rotation, and constrain the underside of the C7 cervical spine [19].

Table 1
Material properties and element types in the model.

Components	Young, s Modulus (MPa)	Poisson Ratio	Element type
Bone	$\rho = 47 + 1.122 * HU$ $E = 0.69 * \hat{\rho 1.35}$	0.3	C3D4
Endplate	500	0.4	C3D8RH
Facet cartilage	10.4	0.4	C3D8RH
Nucleus pulposus	Mooney − Rivlin C10 = 0.12 C1 = 0.09		C3D8RH
Annulus ground	Mooney − Rivlin C10 = 0.56 C1 = 0.14		C3D8RH
Fiber	450	0.45	Rod
Ligaments	stress–strain curves		Spring
Cage(Ti6Al4V)	110000	0.3	C3D4
Bone graft cage	3500	0.3	C3D4

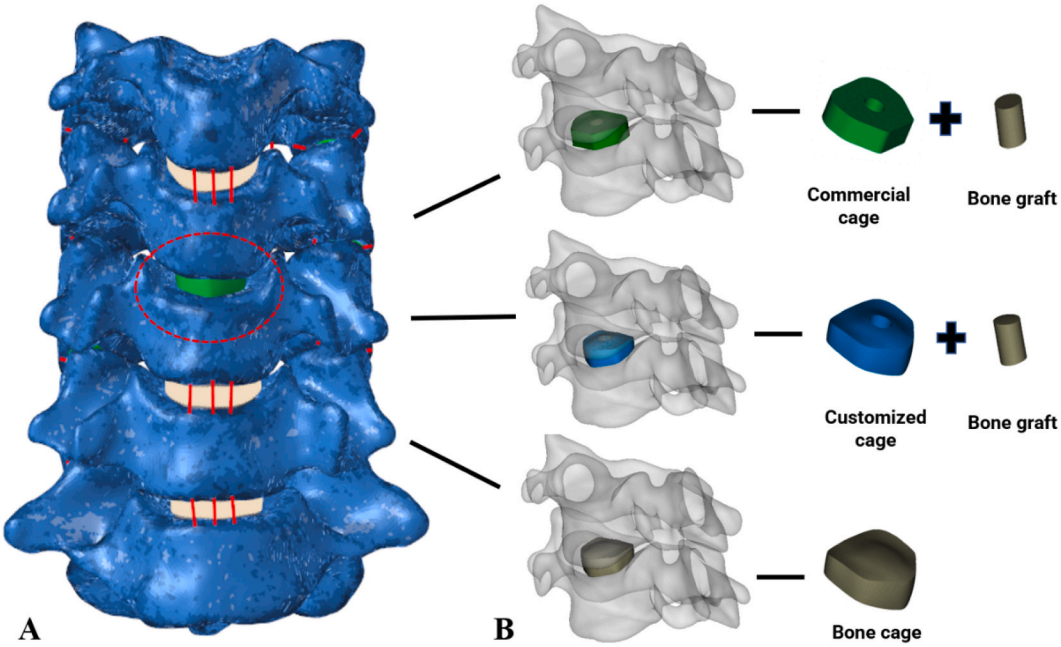

Fig. 2. 3D view of implants used in ACDF models (A) ACDF model and (B) Three cage models and bone implants assembled in ACDF models.

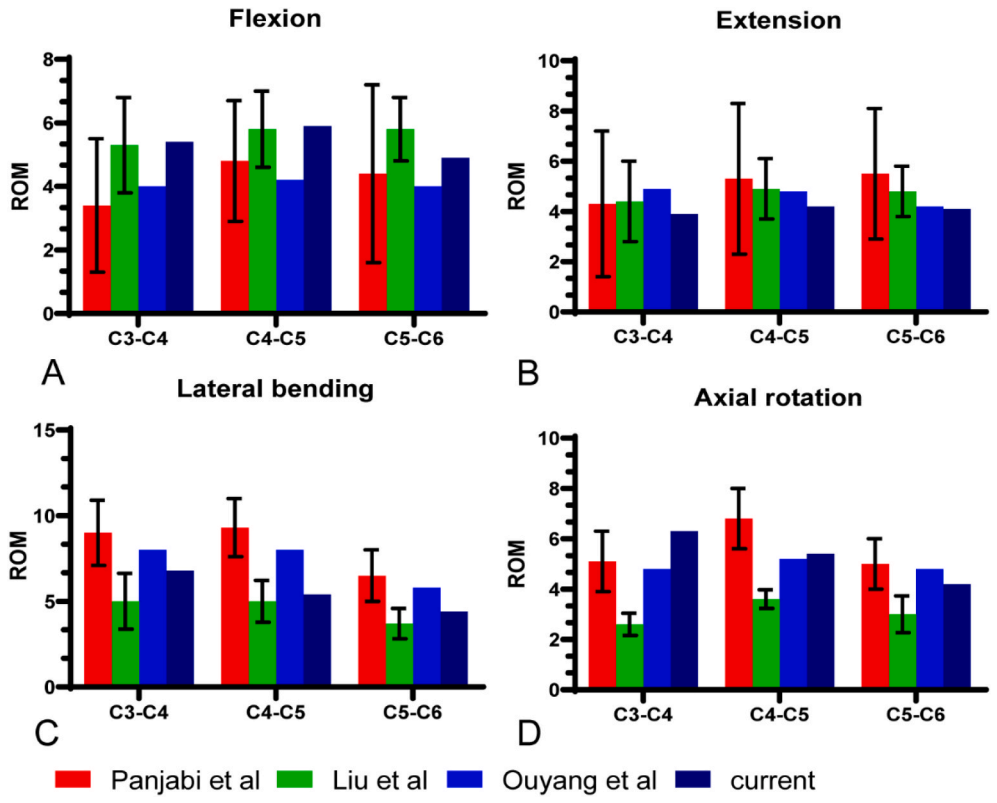

Fig. 3. Validation of the C3-7 intact model. (A)Flexion. (B)Extension. (C)Lateral bending. (D)Axial rotation.

The cage-bone interface used surface-to-surface contact, setting the friction coefficient to 0.5 [20]. The contact between the vertebral body, intervertebral disc, and endplate was set using the stick set, and the contact of facet joints was set using the slide set.

3. Results

3.1. Model validation

The FEA model in this experiment was compared to a previous experimental model (in vivo or in-vivo) (Fig. 3A–D). The present test complete model yielded a range of motion (ROM) in C3-4, C4-5, and C5-6 segments in forwarding flexion-extension (5.4°, 5.9°, 4.9°/3.9°, 4.2°, and 4.1°), lateral bending (6.8°, 5.4°, and 4.4°), and rotational (6.3°, 5.4°, and 4.2°) conditions, consistent with previous findings. Therefore, the FEA model in the present experimental study was valid [17,21,22].

3.2. ROM

The angular results for the position change were obtained by selecting two points on the same plane on the vertebrae and subtracting the angle of the next vertebrae from the last vertebrae to obtain the ROM value. The ROMs of models A, B, and C at C34, C45, and C56 segments compared to the full model are shown in Table 2. The ROM of the three models increased in C34 and C45 segments in flexion-extension conditions (Fig. 4A and B) and decreased in lateral bending and axial rotation conditions compared to the intact model (Fig. 4C and D).

3.3. von Mises stress for cage-endplate

The peak von Mises stress of the C4 inferior endplate in the three different cages is shown in Fig. 5. Under axial rotation, the commercial cage model showed maximum peak stress of 40.3 MPa. Under flexion, the bone graft cage model showed a minimum peak stress of 11.9 MPa in the inferior endplate of C4.

The peak von Mises stress on the superior endplate of C5 for three different cage models is shown in Fig. 6. Under axial rotation, the commercial cage model showed maximum peak stress of 43.2 MPa. Under the extension, the bone graft cage model showed a minimum peak stress of 9.4 MPa in the superior endplate of C5.

3.4. von Mises stress of cage

The von Mises stress distributions of the three cage models in ACDF are shown in Fig. 7. The stresses on the commercial cage model were more concentrated on the surface area, while the stresses on the customized cage model and bone graft cage model were more widely distributed across the cage surface. The maximum peak stress of the customized cage model and the bone graft cage model was lower than that of the commercial cage model under flexion, extension, lateral bending, and axial rotation. The commercial cage model showed a maximum stress of 709.3 MPa under lateral bending; the customized cage model showed a maximum stress of 196.8 MPa under axial rotation, and the bone graft cage model showed a maximum stress of 117.3 MPa under lateral bending. The maximum stress was mainly concentrated at the junction of the endplate and the edges of the cage model.

3.5. von Mises stress of bone graft

Fig. 8 shows the maximum von Mises stress in bone grafts in the commercial cage model and customized cage model. In both cases, the bone graft experienced maximum force under lateral bending movement, followed by axial rotation, flexion, and extension. The maximum stress in lateral bending conditions was 5.5 MPa and 1.5 MPa for custom cage bone implants and commercial cage bone implants, respectively. The maximum stress on the bone graft was observed at the margin of contact with the cage.

4. Discussion

The ACDF procedure using an intervertebral fusion cage for fixation is a classic surgical approach for the anterior cervical spine, as

Table 2
Percentage change in ROM for different cages relative to the intact model.

Flexion			Extension			Lateral bending			Axial rotation		
C34	C45	C56	C34	C45	C56	C34	C45	C56	C34	C45	C56
5.4	5.9	4.9	3.9	4.2	4.1	6.8	5.4	4.4	6.3	5.4	4.2
4.4%	− 96.2%	40.0%	2.8%	− 98.0%	40.2%	− 22.0%	− 96.2%	− 28.4%	− 22.2%	− 96.6%	− 29.7%
4.6%	− 97.4%	40.0%	2.8%	− 98.5%	40.0%	− 22.5%	− 97.0%	− 29.0%	− 22.5%	− 98.3%	− 30.0%
4.4%	− 96.0%	39.7%	2.5%	− 96.9%	40.0%	− 21.6%	− 95.0%	− 27.7%	− 21.7%	− 95.1%	− 28.3%

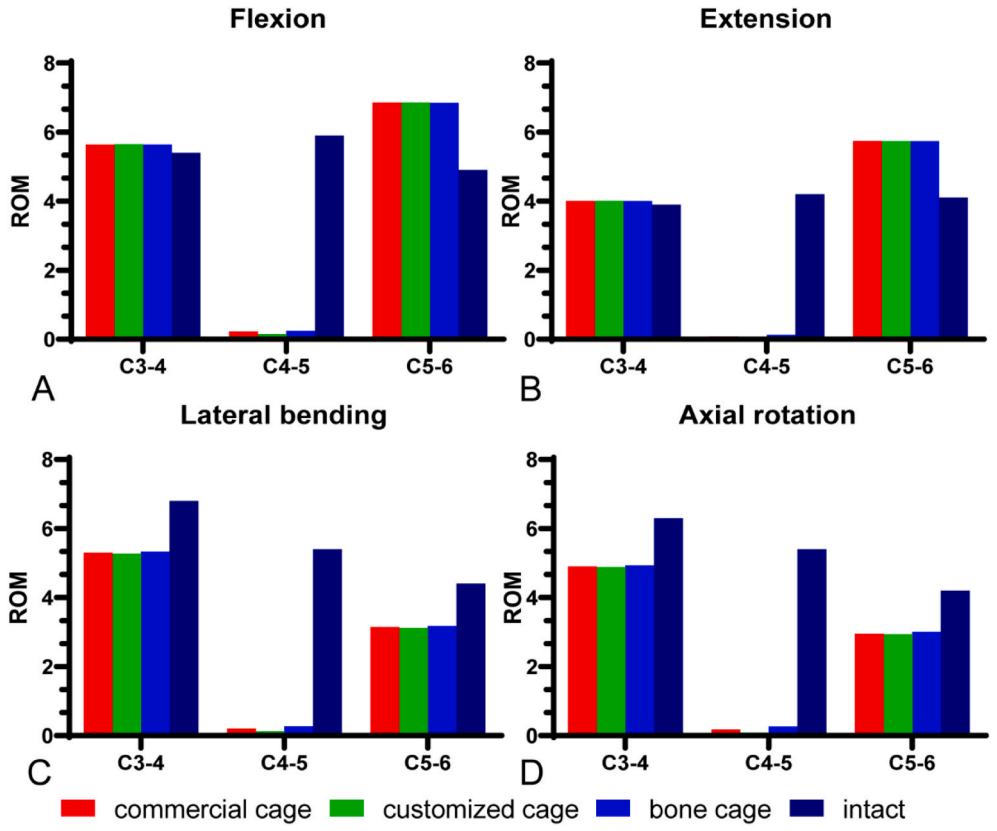

Fig. 4. ROM comparison for three different cages working conditions. (A)Flexion. (B)Extension. (C)Lateral bending. (D)Axial rotation.

it supports the vertebral space, restores intervertebral height, and maintains vertebral stability [3,4]. Nevertheless, the mismatch between the cage and the vertebral body after surgery and the excessive elastic modulus often lead to postoperative complications, including cage subsidence, adjacent intervertebral disc degeneration, and bone non-union [23]. Previous studies have shown that bionic implants can better distribute stress [13,21], however, only a few reports of custom anatomical intervertebral fusions are available and the benefits of bionic implants have not been quantified. In this work, we evaluated the advantages of using personalized data from the cervical spine to build a bionic cage, validated its impact on the biomechanics of adjacent segments after ACDF, and compared it to a conventional cage.

Post-ACDF intervertebral fusion cage and endplate contact are essential as they influence the emergence of subsidence. The surgical scraping off of a part of the endplate enables a proper fit of the intervertebral fusion to the vertebral body. Unsuitable interbody fusion and untrimmed endplate contact result in an unreasonable distribution of stress concentration, leading to stress shielding and the occurrence of subsidence [24]. Therefore, better contact between the intervertebral fusion cage and end plate and reduction of unreasonable matching are research hot spots in the field. Wang et al. [25] designed several types of cages, like rectangular, kidney, and 12-leaf-shaped. They simulated the anterior cervical plate and cage surgery to compare the biomechanical effects of all cages and found that the 12-leaf cage had a more desirable effect in resisting the onset of postoperative subsidence. Li et al. [26] had also designed a porous fusion cage by local topological optimization, which enhanced the osseointegration effect but, at the macroscopic level, was still limited to a neat structure. The experiment focused only on cage shape optimization, without considering the state of the cage fit to the upper and lower endplates, and did not accurately provide a good assessment of the cage-bone contact surface. Zhang et al. [13] also designed an end-plate compliant cage and demonstrated the reduction in stresses at the cage-bone interface and adjacent joints compared to conventional cages. Therefore, the von Mises size and distribution of the cage-bone interface may impact the occurrence of postoperative cage subsidence.

In this work, we implanted three cages into the ACDF surgical model to obtain the stress distribution of adjacent endplates. The commercial cage showed the maximum von Mises stress area in the inferior endplate of C4 and the superior endplate of C5 under rotation. This may be attributed to the stress concentration caused due to the mismatch between the endplate and the cage under rotation. The commercial cage has a uniform design and cannot be well adapted to all patients. Thus, the high-stress concentration area is generated. Under all motions, the bone graft cage had lower maximum stress and a more uniform stress distribution compared to the other two cages from the C45 upper and lower endplates. The maximum von Mises stress peaked at 40.3 MPa and 43.2 MPa in the lower endplate on C4 and the upper endplate on C5 in the commercial cage under rotation. Compared to the commercial cage, the customized and bone cages showed a 26.3% and 41.2% reduction in peak stress on the upper endplate at c5, respectively. The

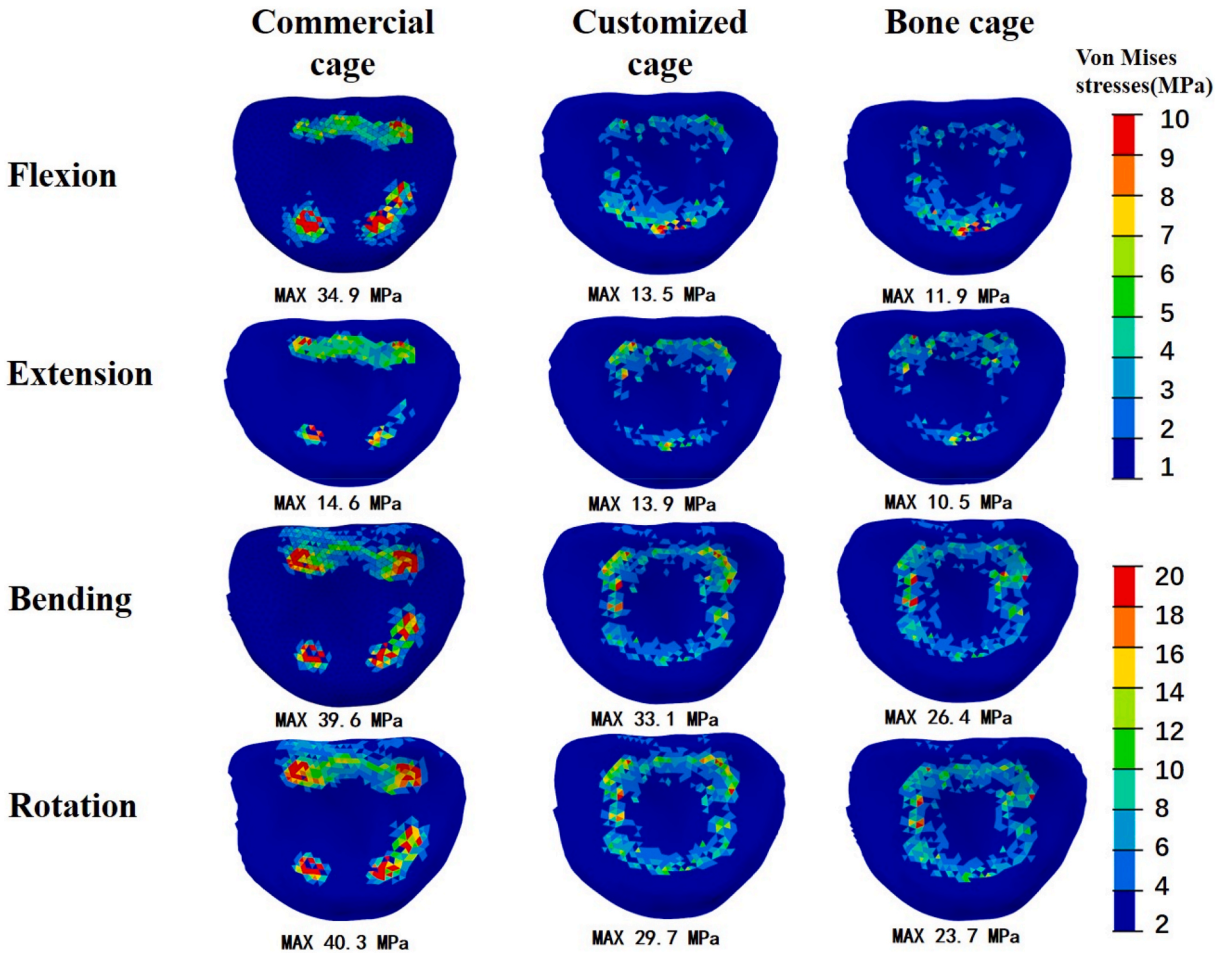

Fig. 5. The von Mises stress distribution diagram and maximum von Mises stress on inferior endplate for different cages under flexion, extension, bending, and rotation conditions.

customized cage was shaped for greater integration into the vertebral body, optimizing the mechanical transfer. In contrast, the bone cage had the lowest stress peaks due to the elastic modulus of the more closely fitting bone. The remaining three working conditions had a similar stress peak trend as the rotating condition. Loenen et al. [27] similarly designed patient-specific trussed lumbar intervertebral fusion cages and obtained a better mechanical distribution on the cage surface, following the same trend as in the present experiment. The commercial cage is not designed to conform to the endplate morphology, creating a localized stress peak due to compression with the endplate during vertebral movement. The primary role of the commercial cage commonly used in clinical practice is the restoration of the intervertebral height and supporting the vertebral body [28,29]. However, patients with commercial cage implants show different outcomes, frequently, subsidence and non-healing bone complications. Figs. 5 and 6 show the stresses on the endplate after implantation with a commercial cage when simulating ACDF. The high-stress concentration areas were greater in the endplate than in the customized cage. After postoperative movement of the vertebral body, a mismatch between the endplate and the cage resulted in compression leading to high-stress concentration, making subsidence complications more likely. The customized cage for an individual patient, with a fitted design adjacent to the vertebrae, matched the surface undulation of the endplate, enabling a preferred stress distribution across the endplate. The customized cage was designed for higher anatomical compatibility, which avoided compression of the cage against the end plate during movement and reduced the risk of subsidence. Zhang et al. [13] also implanted an endplate-conformed cage and a non-conformed cage in cadaveric C45 for biomechanical comparison and found that the former showed a maximum change in mobility during rotation and a lower and more uniform distribution of interfacial stress than the latter. These findings were consistent with our observations of maximum stress peaks under rotation. The change in rotation is more likely to affect the contact between the cage and the end plate, leading to stress concentration. The personalized design is a macroscopic optimization of the cage shape, improving the contact surface and stress distribution. Hence, both customized cage and bone graft cage can effectively reduce the occurrence of postoperative cage subsidence owing to their high endplate compliance and small von Mises stress maxima in the upper and lower endplates compared to the commercial cage, thus effectively reducing the stress at the cage-bone interface.

The stress stimulation of the bone graft implanted in the cage critically affects postoperative bone healing. Appropriate stress

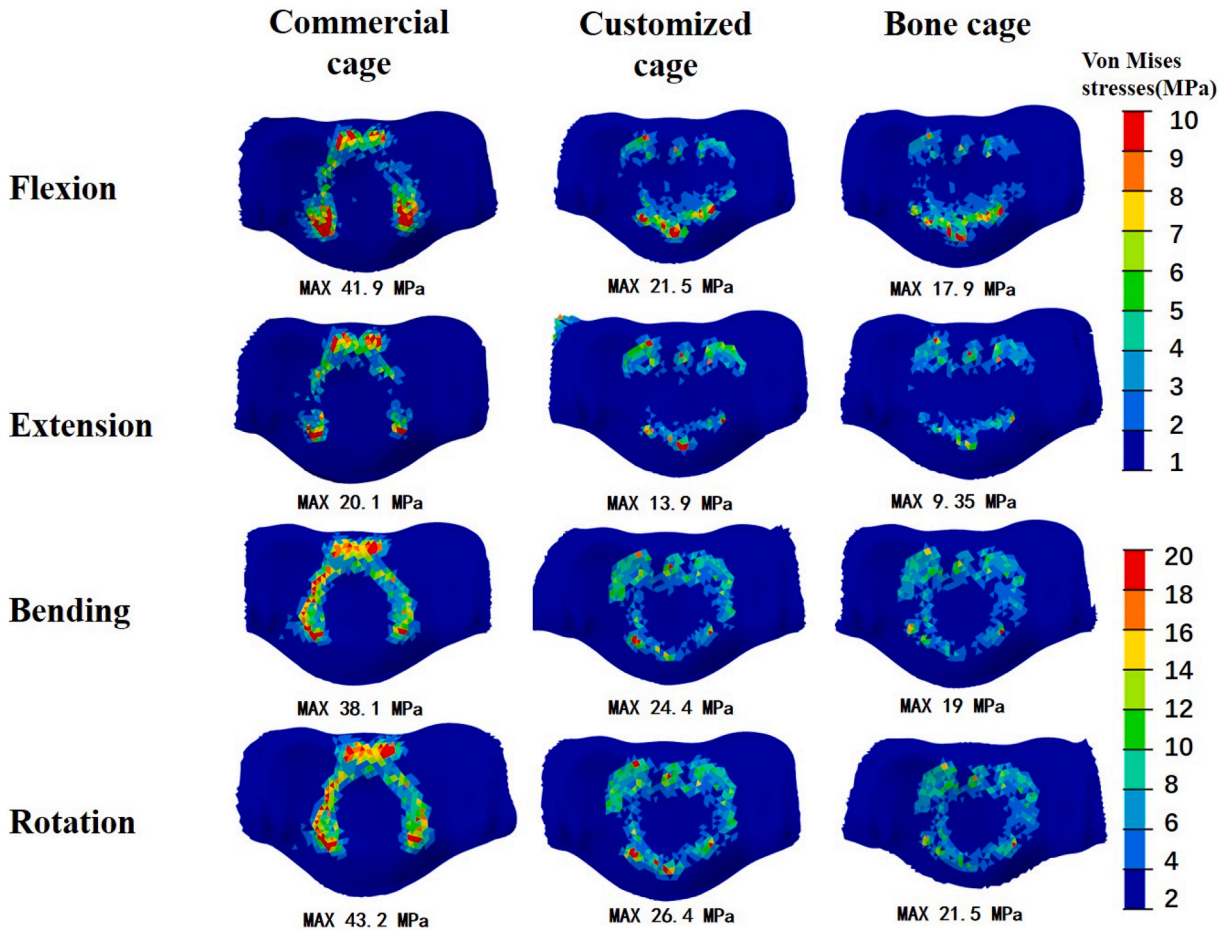

Fig. 6. The von Mises stress distribution diagram and maximum von Mises stress on superior endplate for different cages under flexion, extension, bending, and rotation conditions.

stimulation of the bone graft accelerates bone growth and better bridges the postoperative segmental fusion [30]. Fig. 8 shows that stresses in the bone graft were higher in the customized cage compared to the commercial cage under different working conditions, probably due to the uniform distribution of stresses in the customized cage, which reduced stress shielding and allowed for better transfer of stresses to the bone graft. The maximum stresses were all distributed at the point of contact with the cage, which explained the transfer of stresses on the cage to the bone graft.

The influence of cage subsidence is multifactorial and affected not only by the stresses applied to the superior and inferior endplate surfaces but also by the stress concentrations due to high stresses on the cage, thus affecting bone healing and slowing down the segmental fusion [31,32]. An inappropriate cage during ACDF poses a greater risk. The Jayanta study found that using ACDF and total disc replacement (TDR), respectively, with different bone qualities, revealed that TDR was better at reducing stress in the adjacent segment when the patient's bone quality was poor [33]. Therefore, the cage application or procedure choice can be based on the patient's condition. As the main bridge between the upper and lower vertebrae, a suitable intervertebral fusion cage is essential to post-operative recovery [34,35]. High stresses concentrated on the cage surface may lead to subsidence [12,36]. Therefore, effectively reducing the stress on the cage and stress concentrations, for a more uniform stress distribution on the cage to maintain a positive stimulation effect on bone growth, is a research hotspot [37– 39]. In this experiment, the commercial cage showed the maximum von Mises stress peak under all working conditions compared to other cages, and a stress concentration zone in the contact area with the endplate was observed (Fig. 7). The customized cage and bone graft cage are anatomically designed to better fit the endplate and maximize the contact area with the endplate, resulting in more uniform force transfer and distribution on the cage. The customized cage offered the advantage of actively matching the cervical segment to other conventional cages without the need for extensive destruction of the cartilage endplates to accommodate the cage. Moreover, the bionic cage design shows better synergy with the upper and lower vertebrae during vertebral movements, with forces being evenly transferred from the vertebrae to the cage, leading to an optimized design.

The commercial cage showed a maximum von Mises stress peak at 709.3 MPa in the bending condition, much higher than the 175.3 MPa and 117.3 MPa in the customized cage and bone graft cage, respectively. During bone healing, the stiffness of the new bone

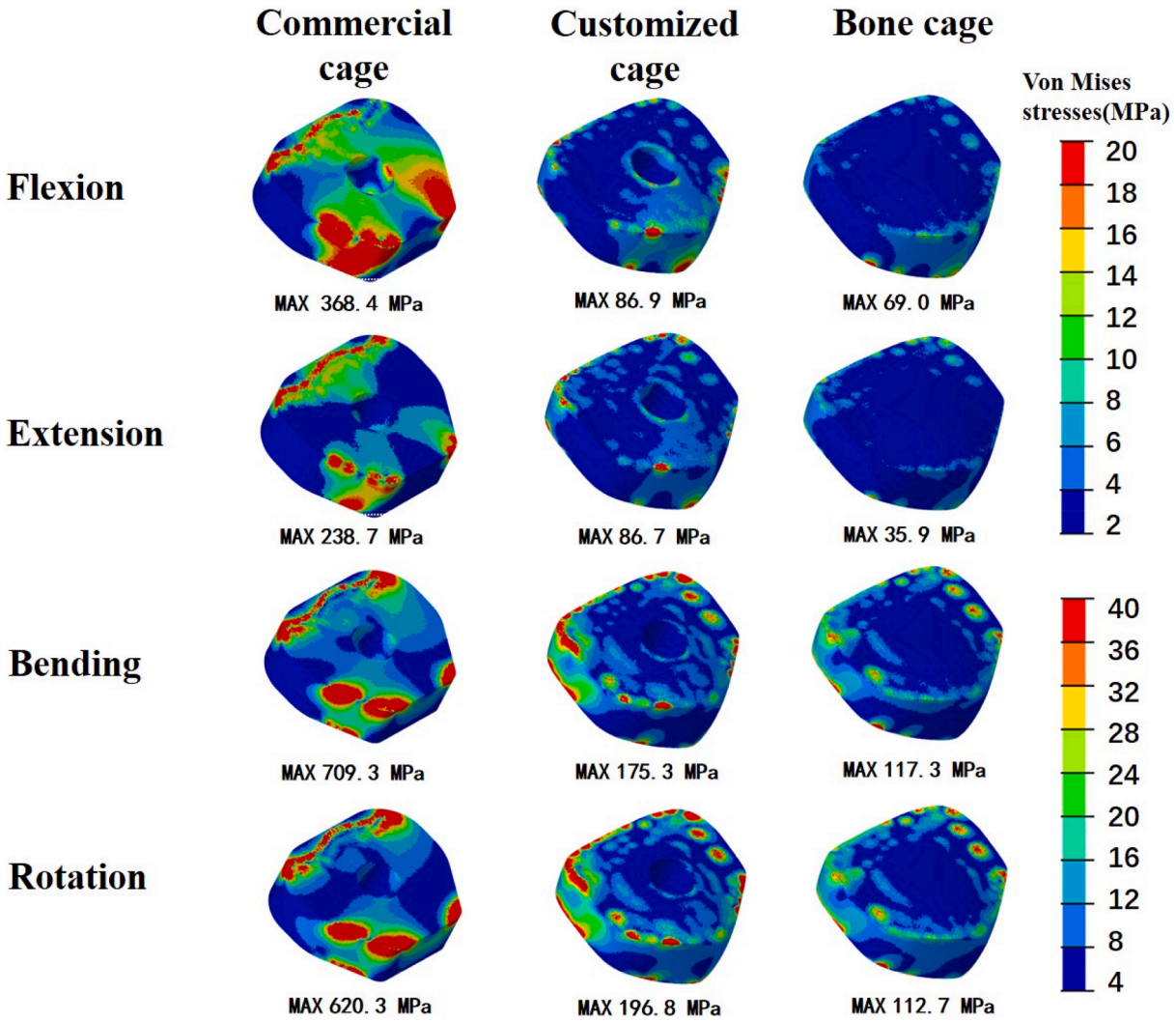

Fig. 7. The von Mises stress distribution diagram and maximum von Mises stress for different cages under flexion, extension, bending, and rotation conditions.

adjacent to the cage increases as it hardens, and some of the stresses on the cage are transferred to the new bone thereby stimulating bone growth [40]. Therefore, high-stress concentration in the commercial cage may fail in better stress transfer, thus prolonging the bone healing time and increasing the chance of subsidence. Both the customized and bone graft cage showed low-stress peaks with positive force conductivity. The two cages were optimized to the vertebral structure but the stresses applied were different, with the bone graft cage having a lower stress peak than the customized cage. This may be because the bone graft cage had a lower modulus of elasticity than the customized cage, which was close to the modulus of bone and more suited for mechanical conduction between the vertebrae. The peak von Mises stresses were much higher in all three cages in both the lateral bending and rotating conditions compared to the other two motions, indicating that excessive stresses were more likely to occur in the cages in these two motions, resulting in stress shielding. Both movement patterns can be reduced during the postoperative recovery period to avoid excessive stress between the cage and the vertebral body, which can affect the fusion. The customized cage is an upgrade on the commercial cage design, compensating for some of the mismatches at the intersection. After a sensible profile design, incorporating material changes and micro-pores will be pivotal in addressing post-operative subsidence.

An unsuited intervertebral fusion not only affects the stress profile of the adjacent vertebrae but also predisposes the adjacent segment to degeneration after surgery. The degeneration of adjacent segments of the cervical spine may be due to the changes in the nucleus pulposus. During the degeneration, the nucleus pulposus alters from the liquid phase into a solid phase and the elastic modulus gradually approaches that of the disc matrix, leading to biomechanical alterations [41,42]. The ROM is commonly used in studies of the interbody fusion cage to evaluate the altered motion of the cervical spine and its effects on the compensation of the adjacent segments [17,18,22]. For post-surgical cervical segmental fusion fixation, the mobility of the adjacent cervical segment usually tends to increase to substitute for the reduction in the fixed one to maintain normal life activities. As shown in Table 2, the ROM of the C45

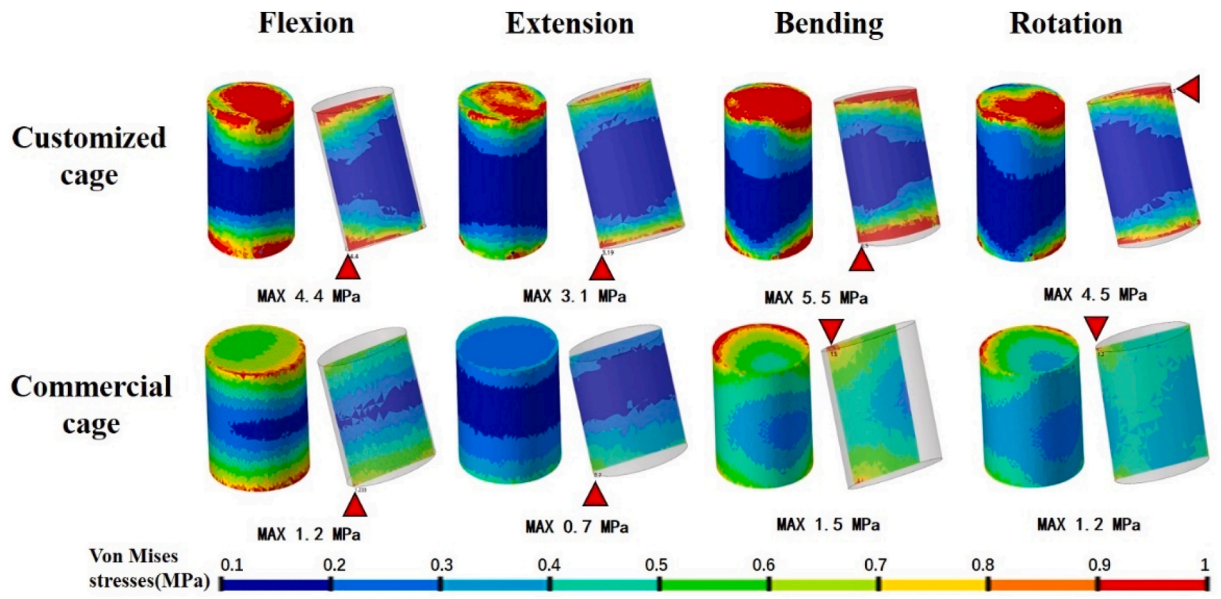

Fig. 8. Stress distribution and peak stresses of bone grafts in customized and commercial cages under flexion, extension, bending, and rotation conditions.

segment decreased significantly in the three cage models due to the fused fixation of this segment. The bionic design of the customized cage reduced the relative motion of the vertebral body during movement. The customized cage had the greatest percentage reduction in ROM values at the C45 segment, which provides the optimum fixation for segmental fusion. However, the bone cage has a larger ROM value in the C45 segment than the commercial cage, which might be due to the modulus of elasticity factor of the bone cage resulting in deformation during vertebral motion. The ROMs of C34 and C56 showed a compensatory increase in anterior flexion and posterior extension, enhancing the stress on adjacent segments, and making them more susceptible to degeneration. The same phenomenon has been reported previously [20,43,44]. Li et al. [45] used FEA to compare the effects of two different plate fixations on the spine. The ROM of adjacent segments showed a compensatory increase but decreased under lateral bending and rotation conditions. The implant affected the mobility of the adjacent segment, thus impacting the degeneration of the adjacent segment. Furthermore, in the C45 segment, the customized cage fused better than the other two cages because its design was better suited to the upper and lower endplates and more anatomically accurate. However, the fusion rate of the bone graft cage with the same profile differed from that of the customized one, probably because the difference in modulus of elasticity also affected the fusion rate.

This study has some limitations that warrant consideration. First, the cervical spine is complex, and the present FEA model has limitations and simplifications that do not consider the influence that muscles may have on the movement and stress of the cervical spine. Second, the cage model was designed to be solid, ignoring the mesh for better convergence of the model's calculations. Despite these limitations, the present study ensured that the conditions of the model were consistent with those described in the literature and effectively demonstrated the biomechanical changes in the personalized cage model after ACDF surgery. With advances in bone engineering and biomechanics, incorporating a lattice structure based on the patient's design, which not only maintains structural advantages but also lightens it and reduces the equivalent elastic modulus, is possible. The lattice also aids bone tensioning, allowing for rapid postoperative vertebral body fusion.

5. Conclusions

Herein, the relationship between different postoperative cages and cervical spine biomechanics was successfully determined based on the ACDF surgical model and different intervertebral fusion cage models. The customized design provided a more uniform stress distribution over the intervertebral fusion cage while avoiding high-stress concentrations on the endplate and reducing the occurrence risk of post-operative cage subsidence. The customized cage also reduced the impact on adjacent segmented disc degeneration and accelerated bone healing with a higher mechanical stimulation of the bone graft.

Author contribution statement

Bin Sun: Conceived and designed the experiments; Performed the experiments; Wrote the paper.
Qing Han; JinCheng Wang: Analyzed and interpreted the data.
Fengxu Sui; Yang Liu: Contributed reagents, materials, analysis tools or data.
AoBo Zhang: Performed the experiments.

Peng Xia: Conceived and designed the experiments.
XiaoYu Yang: Conceived and designed the experiments; Analyzed and interpreted the data.

Funding statement

Dr Xiaoyu Yang was supported by Department of Finance of Jilin Province [2019SCTZ002].
This work was supported by National Natural Science Foundation of China [82072456 and 82272504], National Key R&D Program of China [2018YFB1105100], Department of Science and Technology of Jilin Province [20200404202YY, 20200403086SF, 20200201453JC, 202201ZYTS505, and 20200404137YY], Department of Finance of Jilin Province [2019SCZT046 and 2020SCZT037], Undergraduate teaching reform research project of Jilin University [4Z2000610852].

Data availability statement

Data will be made available on request.

Declaration of interest's statement

The authors declare no conflict of interest.

References

[1] Z. Ghogawala, Anterior cervical option to manage degenerative cervical myelopathy, Neurosurg. Clin. 29 (1) (2018) 83–89, https://doi.org/10.1016/j.nec.2017.09.005.
[2] B. Peng, M.J. DePalma, Cervical disc degeneration and neck pain, J. Pain Res. 11 (2018) 2853–2857, https://doi.org/10.2147/JPR.S180018.
[3] M.K. Kim, S.M. Kim, K.M. Jeon, T.S. Kim, Radiographic comparison of four anterior fusion methods in two level cervical disc diseases: autograft plate fixation versus cage plate fixation versus stand-alone cage fusion versus corpectomy and plate fixation, J Korean Neurosurg. Soc. 51 (3) (2012) 135–140, https://doi.org/10.3340/jkns.2012.51.3.135.
[4] A. Chien, D.M. Lai, S.F. Wang, W.L. Hsu, C.H. Cheng, J.L. Wang, Comparison of cervical kinematics, pain, and functional disability between single- and two-level anterior cervical discectomy and fusion, Spine (Phila Pa 1976) 41 (15) (2016) E915–E922, https://doi.org/10.1097/BRS.0000000000001502.
[5] B. Ren, W. Gao, J. An, M. Wu, Y. Shen, Risk factors of cage nonunion after anterior cervical discectomy and fusion, Medicine 99 (12) (2020), https://doi.org/10.1097/md.0000000000019550.
[6] N. Bocahut, E. Audureau, A. Poignard, et al., Incidence and impact of implant subsidence after stand-alone lateral lumbar interbody fusion, Orthop. Traumatol.-Surg. Res. 104 (3) (2018) 405–410, https://doi.org/10.1016/j.otsr.2017.11.018.
[7] C. Caparros, J. Guillem-Marti, M. Molmeneu, M. Punset, J.A. Calero, F.J. Gil, Mechanical properties and in vitro biological response to porous titanium alloys prepared for use in intervertebral implants, J. Mech. Behav. Biomed. Mater. 39 (2014) 79–86, https://doi.org/10.1016/j.jmbbm.2014.05.029.
[8] R. Opsenak, M. Hanko, P. Snopko, K. Varga, B. Kolarovszki, Subsidence of anchored cage after anterior cervical discectomy, Bratislava Med. J.-Bratislavske Lekarske Listy 120 (5) (2019) 356–361, https://doi.org/10.4149/bll_2019_058.
[9] P.B. Suh, C. Puttlitz, C. Lewis, B.S. Bal, K. McGilvray, The effect of cervical lnterbody cage morphology, material composition, and substrate density on cage subsidence, J. Am. Acad. Orthop. Surg. 25 (2) (2017) 160–168, https://doi.org/10.5435/jaaos-d-16-00390.
[10] J.-H. Tan, C.K. Cheong, H.W.D. Hey, Titanium (Ti) cages may be superior to polyetheretherketone (PEEK) cages in lumbar interbody fusion: a systematic review and meta-analysis of clinical and radiological outcomes of spinal interbody fusions using Ti versus PEEK cages, Eur. Spine J. 30 (5) (2021) 1285–1295, https://doi.org/10.1007/s00586-021-06748-w.
[11] Y.-C. Yao, P.-H. Chou, H.-H. Lin, S.-T. Wang, M.-C. Chang, Outcome of Ti/PEEK versus PEEK cages in minimally invasive transforaminal lumbar interbody fusion, Global Spine J. (2021), https://doi.org/10.1177/21925682211000323.
[12] H. Wang, Y. Wan, Q. Li, et al., Porous fusion cage design via integrated global-local topology optimization and biomechanical analysis of performance, J. Mech. Behav. Biomed. Mater. 112 (2020), 103982, https://doi.org/10.1016/j.jmbbm.2020.103982.
[13] F. Zhang, H.C. Xu, B. Yin, et al., Can an endplate-conformed cervical cage provide a better biomechanical environment than a typical non-conformed cage?: a finite element model and cadaver study, Orthop. Surg. 8 (3) (2016) 367–376, https://doi.org/10.1111/os.12261.
[14] J. Kang, E. Dong, X. Li, et al., Topological design and biomechanical evaluation for 3D printed multi-segment artificial vertebral implants, Mater. Sci. Eng. C Mater. Biol. Appl. 127 (2021), 112250, https://doi.org/10.1016/j.msec.2021.112250.
[15] U.M. Ayturk, C.M. Puttlitz, Parametric convergence sensitivity and validation of a finite element model of the human lumbar spine, Comput. Methods Biomech. Biomed. Eng. 14 (8) (2011) 695–705, https://doi.org/10.1080/10255842.2010.493517.
[16] J.Y. Rho, M.C. Hobatho, R.B. Ashman, Relations of mechanical properties to density and CT numbers in human bone, Med. Eng. Phys. 17 (5) (1995) 347–355.
[17] P. Ouyang, T. Lu, X. He, Z. Gao, X. Cai, Z. Jin, Biomechanical comparison of integrated fixation cage versus anterior cervical plate and cage in anterior cervical corpectomy and fusion (ACCF): a finite element analysis, Med. Sci. Mon. Int. Med. J. Exp. Clin. Res. 25 (2019) 1489–1498, https://doi.org/10.12659/MSM.913630.
[18] T.K. Wu, Y. Meng, B.Y. Wang, et al., Biomechanics following skip-level cervical disc arthroplasty versus skip-level cervical discectomy and fusion: a finite element-based study, BMC Muscoskel. Disord. 20 (1) (2019) 49, https://doi.org/10.1186/s12891-019-2425-3.
[19] D. Ganbat, Y.H. Kim, K. Kim, Y.J. Jin, W.M. Park, Effect of mechanical loading on heterotopic ossification in cervical total disc replacement: a three-dimensional finite element analysis, Biomech. Model. Mechanobiol. 15 (5) (2016) 1191–1199, https://doi.org/10.1007/s10237-015-0752-3.
[20] M. Lin, S.Z. Shapiro, J. Doulgeris, E.D. Engeberg, C.T. Tsai, F.D. Vrionis, Cage-screw and anterior plating combination reduces the risk of micromotion and subsidence in multilevel anterior cervical discectomy and fusion-a finite element study, Spine J. 21 (5) (2021) 874–882, https://doi.org/10.1016/j.spinee.2021.01.015.
[21] J. Liu, R. Wang, H. Wang, et al., Biomechanical comparison of a new memory compression alloy plate versus traditional titanium plate for anterior cervical discectomy and fusion: a finite element analysis, BioMed Res. Int. 2020 (5) (2020) 1–10.
[22] M.M. Panjabi, J.J. Crisco, A. Vasavada, et al., Mechanical properties of the human cervical spine as shown by three-dimensional load-displacement curves, J. Bone Jt. Surg. Am. Vol. 58 (5) (1976) 642–652.
[23] N.E. Epstein, A review of complication rates for anterior cervical diskectomy and fusion (ACDF), Surg. Neurol. Int. 10 (2019) 100, https://doi.org/10.25259/SNI-191-2019.
[24] T. Amorim-Barbosa, C. Pereira, D. Catelas, et al., Risk factors for cage subsidence and clinical outcomes after transforaminal and posterior lumbar interbody fusion, Eur. J. Orthop. Surg. Traumatol. (2021), https://doi.org/10.1007/s00590-021-03103-z.

[25] J. Wang, Z. Qian, L. Ren, Biomechanical comparison of optimal shapes for the cervical intervertebral fusion cage for C5-C6 cervical fusion using the anterior cervical plate and cage (ACPC) fixation system: a finite element analysis, Med. Sci. Mon. Int. Med. J. Exp. Clin. Res. 25 (2019) 8379–8388, https://doi.org/10.12659/MSM.918489.
[26] N. Li, et al., Porous interbody fusion cage design via topology optimization and biomechanical performance analysis, Comput. Methods Biomech. Biomed. Eng. (2022) 1–10, https://doi.org/10.1080/10255842.2022.2081505.
[27] A.C.Y. Loenen, et al., Patient-specific variations in local strain patterns on the surface of a trussed titanium interbody cage, Front. Bioeng. Biotechnol. 9 (2021), 750246.
[28] W. Yuan, A.-K. Kaliya-Perumal, S.M. Chou, J.Y.-L. Oh, Does lumbar interbody cage size influence subsidence? A biomechanical study, Spine 45 (2) (2020) 88–95, https://doi.org/10.1097/brs.0000000000003194.
[29] S. Rastegar, P.-J. Arnoux, X. Wang, C.-E. Aubin, Biomechanical analysis of segmental lumbar lordosis and risk of cage subsidence with different cage heights and alternative placements in transforaminal lumbar interbody fusion, Comput. Methods Biomech. Biomed. Eng. 23 (9) (2020) 456–466, https://doi.org/10.1080/10255842.2020.1737027.
[30] P.S. Manickam, S. Roy, G.M. Shetty, Biomechanical evaluation of a novel S-type, dynamic zero-profile cage design for anterior cervical discectomy and fusion with variations in bone graft shape: a finite element analysis, World Neurosurg. (2021), https://doi.org/10.1016/j.wneu.2021.07.013.
[31] N.Z. Zhang, Q.S. Xiong, J. Yao, B.L. Liu, M. Zhang, C.K. Cheng, Biomechanical changes at the adjacent segments induced by a lordotic porous interbody fusion cage, Comput. Biol. Med. 143 (2022), 105320, https://doi.org/10.1016/j.compbiomed.2022.105320.
[32] A.C.Y. Loenen, J. Noailly, K. Ito, P.C. Willems, J.J. Arts, B. van Rietbergen, Patient-specific variations in local strain patterns on the surface of a trussed titanium interbody cage, Front. Bioeng. Biotechnol. 9 (2021), 750246, https://doi.org/10.3389/fbioe.2021.750246.
[33] J.K. Biswas, et al., Effects of cervical disc replacement and anterior fusion for different bone conditions: a finite element study, Int. J. Multiscale Comput. Eng. 17 (4) (2019) 411–427.
[34] J. Hakalo, C. Pezowicz, J. Wronski, R. Bedzinski, M. Kasprowicz, Comparative biomechanical study of cervical spine stabilisation by cage alone, cage with plate, or plate-cage: a porcine model, J. Orthop. Surg. (Hong Kong) 16 (1) (2008) 9–13, https://doi.org/10.1177/230949900801600103.
[35] J. Wu, D. Luo, X. Ye, X. Luo, L. Yan, H. Qian, Anatomy-related risk factors for the subsidence of titanium mesh cage in cervical reconstruction after one-level corpectomy, Int. J. Clin. Exp. Med. 8 (5) (2015) 7405–7411.
[36] W. Fan, L.X. Guo, M. Zhang, Biomechanical analysis of lumbar interbody fusion supplemented with various posterior stabilization systems, Eur. Spine J. 30 (8) (2021) 2342–2350, https://doi.org/10.1007/s00586-021-06856-7.
[37] H. Wang, Y. Wan, Q. Li, et al., Porous fusion cage design via integrated global-local topology optimization and biomechanical analysis of performance, J. Mech. Behav. Biomed. Mater. 112 (2020), https://doi.org/10.1016/j.jmbbm.2020.103982.
[38] P. Li, W. Jiang, J. Yan, et al., A novel 3D printed cage with microporous structure and in vivo fusion function, J. Biomed. Mater. Res. 107 (7) (2019) 1386–1392, https://doi.org/10.1002/jbm.a.36652.
[39] A. Calvo-Echenique, J. Cegonino, A. Perez Del Palomar, Is there any advantage of using stand-alone cages? A numerical approach, Biomed. Eng. Online 18 (1) (2019) 63, https://doi.org/10.1186/s12938-019-0684-8.
[40] V.A.S. Ramakrishna, U. Chamoli, A.G. Larosa, S.C. Mukhopadhyay, B.G. Prusty, A.D. Diwan, Finite element modeling of temporal bone graft changes in XLIF: quantifying biomechanical effects at adjacent levels, J. Orthop. Res. (2021), https://doi.org/10.1002/jor.25166.
[41] J.C. Iatridis, L.A. Setton, M. Weidenbaum, V.C. Mow, Alterations in the mechanical behavior of the human lumbar nucleus pulposus with degeneration and aging, J. Orthop. Res. 15 (2) (2010) 318–322.
[42] S. Tang, B.J. Rebholz, Does anterior lumbar interbody fusion promote adjacent degeneration in degenerative disc disease? A finite element study, J. Orthop. Sci. 16 (2) (2011) 221–228, https://doi.org/10.1007/s00776-011-0037-3.
[43] J. Sun, Q. Wang, D. Cai, et al., A lattice topology optimization of cervical interbody fusion cage and finite element comparison with ZK60 and Ti-6Al-4V cages, BMC Muscoskel. Disord. 22 (1) (2021) 390, https://doi.org/10.1186/s12891-021-04244-2.
[44] M. Xu, J. Yang, I. Lieberman, R. Haddas, Stress distribution in vertebral bone and pedicle screw and screw-bone load transfers among various fixation methods for lumbar spine surgical alignment: a finite element study, Med. Eng. Phys. 63 (2019) 26–32, https://doi.org/10.1016/j.medengphy.2018.10.003.
[45] X.F. Li, L.Y. Jin, C.G. Liang, H.L. Yin, X.X. Song, Adjacent-level biomechanics after single-level anterior cervical interbody fusion with anchored zero-profile spacer versus cage-plate construct: a finite element study, BMC Surg. 20 (1) (2020) 66, https://doi.org/10.1186/s12893-020-00729-4.